



# Data-driven correction reduced order models for the quasi-geostrophic equations: a numerical investigation

Changhong Mou<sup>a</sup>, Honghu Liu<sup>a</sup>, David R. Wells<sup>b</sup> and Traian Iliescu<sup>a</sup>

<sup>a</sup> Department of Mathematics, Virginia Tech, Blacksburg, VA, USA; <sup>b</sup> Department of Mathematics, University of North Carolina, Chapel Hill, NC, USA

#### **ABSTRACT**

This paper investigates the recently introduced data-driven correction reduced order model (DDC-ROM) in the numerical simulation of the quasi-geostrophic equations. The DDC-ROM uses available data to model the correction term that is generally used to represent the missing information in low-dimensional ROMs. Physical constraints are added to the DDC-ROM to create the constrained data-driven correction reduced order model (CDDC-ROM) in order to further improve its accuracy and stability. Finally, the DDC-ROM and CDDC-ROM are tested on time intervals that are longer than the time interval over which they were trained. The numerical investigation shows that, for low-dimensional ROMs, both the DDC-ROM and CDDC-ROM perform better than the standard Galerkin ROM (G-ROM) and the CDDC-ROM provides the best results.

#### **ARTICLE HISTORY**

Received 5 August 2019 Accepted 26 December 2019

#### **KEYWORDS**

Reduced order model; data-driven model; physical constraints; quasi-geostrophic equations; closure modelling

#### 1. Introduction

Reduced order models (ROMs) for fluid dynamics have been abundantly investigated in recent decades as a way to reduce the computational cost of high resolution numerical schemes. The success of many ROM approaches has already been documented for various scientific and engineering applications, especially for flows that are governed by relatively few recurrent dominant spatial structures; see e.g. Holmes, Lumley, and Berkooz (1996), Galletti et al. (2004), Sapsis and Lermusiaux (2009), Noack, Morzynski, and Tadmor (2011), Hesthaven, Rozza, and Stamm (2015), Quarteroni, Manzoni, and Negri (2015), Ballarin et al. (2016), Gunzburger, Jiang, and Schneier (2017), Perotto et al. (2017), Fick et al. (2018) and references therein.

In this article, the recently proposed data-driven correction ROM (DDC-ROM) and its variants (Xie et al. 2018; Koc et al. 2019; Mohebujjaman, Rebholz, and Iliescu 2019) are investigated in the numerical simulation of a quasi-geostrophic model of the doublegyre wind-driven ocean circulation. The DDC-ROMs fall into the category of hybrid projection/data-driven ROMs (Galletti et al. 2004; Couplet, Basdevant, and Sagaut 2005; Noack, Papas, and Monkewitz 2005; Lu,

Lin, and Chorin 2017; Hijazi et al. 2019). More specifically, in DDC-ROMs, the interactions among the resolved modes are the same as those in the standard Galerkin projection ROMs, while the interactions involving the unresolved modes are learned through a data-driven approach by fitting, e.g. a quadratic ansatz to the data that represents these missing interactions. In the following, we provide a brief derivation of the DDC-ROMs that builds on the standard projection ROMs, and refer to Xie et al. (2018) and Mohebujjaman, Rebholz, and Iliescu (2019) for more details.

To construct the standard projection ROM, we start with a general nonlinear system that has the following weak form<sup>1</sup> in a suitable Hilbert space X:

$$\begin{pmatrix} \bullet \\ u, v \end{pmatrix} = \langle f(u), v \rangle, \quad \forall v \in X,$$
 (1)

where f is a general nonlinear function,  $u \in X$  is the sought solution, and  $(\cdot, \cdot)$  denotes the inner product on X. We assume that system (1) is parameter dependent and/or needs to be simulated for long time intervals. ROMs aim at an efficient and relatively accurate numerical simulation of (1). Next, we use data (snapshots) available for a few parameter values and/or a short time interval to construct orthonormal modes  $\{\varphi_1, \ldots, \varphi_R\}$ , which represent the recurrent

spatial structures, where R is the rank of the snapshot matrix and typically  $R = \mathcal{O}(10^3)$  or even higher. Then, we choose the dominant modes  $\{\varphi_1, \ldots, \varphi_r\}$ , typically with  $r = \mathcal{O}(10)$ , as ROM basis functions. The r-dimensional *Galerkin ROM (G-ROM)* of (1) is obtained by replacing  $\boldsymbol{u}$  with a Galerkin truncation  $\boldsymbol{u}_r = \sum_{j=1}^r a_j \varphi_j$  and restricting  $\boldsymbol{v}$  to the ROM subspace  $\mathbf{X}^r := \operatorname{span}\{\varphi_1, \ldots, \varphi_r\}$ :

$$\begin{pmatrix} \mathbf{u}_r, \boldsymbol{\varphi}_i \end{pmatrix} = \langle f(\boldsymbol{u}_r), \boldsymbol{\varphi}_i \rangle, \quad i = 1, \dots, r.$$
 (2)

In an offline stage, we construct the ROM, and in an online stage, we repeatedly use the G-ROM (2) for all the parameter values and/or the entire time interval of interest.

To construct the *data-driven correction reduced* order model (DDC-ROM) (Xie et al. 2018; Koc et al. 2019; Mohebujjaman, Rebholz, and Iliescu 2019), we use an alternative approach: We start with a new Galerkin truncation,  $\mathbf{u}_R = \sum_{j=1}^R a_j \boldsymbol{\varphi}_j$ . We emphasise that, since  $R = \mathcal{O}(10^3)$  is the rank of the snapshot matrix, the new Galerkin truncation includes all the information in the available data (snapshots). Next, we replace  $\mathbf{u}$  with  $\mathbf{u}_R$  in (1) and project the resulting PDE onto  $\mathbf{X}^r$ :

$$\begin{pmatrix} \mathbf{u}_R, \boldsymbol{\varphi}_i \end{pmatrix} = \langle f(\boldsymbol{u}_R), \boldsymbol{\varphi}_i \rangle, \quad i = 1, \dots, r.$$
 (3)

Since the ROM modes are orthonormal,  $(\mathbf{u}_R^{\bullet}, \mathbf{\varphi}_i) = (\mathbf{u}_r^{\bullet}, \mathbf{\varphi}_i)$ , i = 1, ..., r. Thus, (3) becomes

$$\begin{pmatrix} \mathbf{u}_r, \boldsymbol{\varphi}_i \end{pmatrix} = \langle f(\boldsymbol{u}_R), \boldsymbol{\varphi}_i \rangle, \quad i = 1, \dots, r,$$
 (4)

which can be written as

$$\begin{pmatrix} \mathbf{u}_r, \boldsymbol{\varphi}_i \end{pmatrix} = \left( f(\boldsymbol{u}_r), \boldsymbol{\varphi}_i \right) + \left[ \left( f(\boldsymbol{u}_R), \boldsymbol{\varphi}_i \right) - \left( f(\boldsymbol{u}_r), \boldsymbol{\varphi}_i \right) \right],$$

$$i = 1, \dots, r. \tag{5}$$

The last term on the right-hand side of (5) is a *Correction term* 

Correction = 
$$[(f(u_R), \varphi_i) - (f(u_r), \varphi_i)].$$
 (6)

Thus, (5) can be written as G-ROM + Correction.

We emphasise that (5) is expected to be more accurate than the G-ROM, since the former is constructed from  $u_R$ , whereas the latter is constructed from  $u_r$ , where  $r = \mathcal{O}(10) \ll R = \mathcal{O}(10^3)$ . Note that (5) is not yet a closed system in  $u_r$ , since the Correction term involves  $u_R$ , which lives in a higher-dimensional

space than  $X^r$ . Thus, to obtain from (5) an efficient r-dimensional ROM, we make the ansatz

Correction = 
$$\left[ \left( f(u_R), \varphi_i \right) - \left( f(u_r), \varphi_i \right) \right]$$
  
  $\approx \left( g(u_r), \varphi_i \right),$  (7)

where **g** is a generic function (e.g. polynomial) whose coefficients/parameters still need to be determined. Once **g** is determined, the ROM (5) with the Correction term replaced by **g** yields the *data-driven correction ROM (DDC-ROM)*:

$$\left[ \begin{pmatrix} \bullet \\ u_r, \varphi_i \end{pmatrix} = \left( f(u_r), \varphi_i \right) + \left( g(u_r), \varphi_i \right), \quad i = 1, \dots, r.$$
(8)

To determine the coefficients/parameters of the function **g** used in (8), we use *data-driven modelling* (Peherstorfer and Willcox 2016; Loiseau and Brunton 2018; Brunton and Kutz 2019), i.e. we solve the following *least squares problem*:

$$\min_{\mathbf{g} \text{ parameters }} \sum_{j=1}^{M} \left\| \text{Correction}(t_j) - \left( \mathbf{g}(\mathbf{u}_r(t_j)), \boldsymbol{\varphi}_i \right) \right\|^2.$$
(9)

The numerical investigations in Xie et al. (2018), Koc et al. (2019) and Mohebujjaman, Rebholz, and Iliescu (2019) show that the DDC-ROM (8) is significantly more accurate than the standard G-ROM in the numerical simulation of two test problems: (i) the 1D Burgers equation with a small diffusion coefficient  $\nu = 10^{-3}$ ; and (ii) a 2D flow past a circular cylinder at Reynolds numbers Re = 100, Re = 500, and Re = 1000.

The main goal of this paper is to investigate the new DDC-ROM (8) in the numerical simulation of the quasi-geostrophic equations (QGE), which represent a significantly more difficult test case than the Burgers equation and the 2D flow past a circular cylinder considered in Xie et al. (2018) and Mohebujjaman, Rebholz, and Iliescu (2019). Indeed, for the 2D flow past a circular cylinder with the Reynolds number Re = 1000, the projection of the velocity field onto the first 8 POD modes captures more than 99% of the kinetic energy. In contrast, for the QGE in the parameter regime investigated in Section 3, a much broader range of spatial scales are actively involved in the time evolution of the turbulent fluid field. Indeed, the total amount of kinetic energy captured by the leading POD modes increases much slower for the QGE investigated here: it requires 16 POD modes to capture 90% of the kinetic energy, 37 modes for 95% of the kinetic energy, and 49 modes for 96% of the kinetic energy.

Furthermore, given the challenges posed by the QGE, we investigate two improvements to the DDC-ROM (8): First, we study the role of adding physical constraints to the DDC-ROM (Mohebujjaman, Rebholz, and Iliescu 2019), in which the model for the Correction term in (7) satisfies the same type of physical constraints as those satisfied by the underlying equations; see (25). We also investigate whether modelling the *commutation error*, i.e. the error that appears as a result of interchanging spatial differentiation and ROM spatial filtering (e.g. projection) (Koc et al. 2019), improves the DDC-ROM accuracy. Finally, we study the DDC-ROM when it is trained on a time interval that is shorter than the time interval over which it is tested.

#### 1.1. Connections to previous work

The DDC-ROM belongs to the class of ROM closure models, which model the effect of the truncated ROM modes (i.e.  $\{\varphi_{r+1}, \ldots, \varphi_R\}$ ) on the resolved ROM modes, (i.e.  $\{\varphi_1, \dots, \varphi_r\}$ ). ROM closure models were first proposed in the pioneering work of Lumley and his collaborators (Holmes, Lumley, and Berkooz 1996) and are currently witnessing a dynamic development in several new directions, e.g. ROM spatial filtering, large eddy simulation (LES), and variational multiscale (VMS) (Bergmann, Bruneau, and Iollo 2009; Wang et al. 2012; Baiges, Codina, and Idelsohn 2015; Azaïez, Rebollo, and Rubino 2017; Rebollo et al. 2017), Mori-Zwanzig (MZ) formalism (Parish, Wentland, and Duraisamy 2019), nonlinear autoregression, moving averages with exogenous inputs (NARMAX) (Chorin and Lu 2015; Lu, Lin, and Chorin 2017), multilevel approaches and empirical model reduction (EMR) (Kravtsov, Kondrashov, and Ghil 2005; Majda and Harlim 2012; Kondrashov, Chekroun, and Ghil 2015), data-adaptive harmonic decomposition and multilayer Stuart-Landau models (DAH-MSLM) (Chekroun and Kondrashov 2017; Kondrashov, Chekroun, and Berloff 2018), and the parameterising manifold (PM) approach rooted in the approximation theory of local invariant manifolds (Chekroun, Liu, and Wang 2015; Chekroun, Liu, and McWilliams 2019), to name just a few. Probably the most dynamic development has been

in using available data and machine learning techniques to develop ROM closure models (San and Maulik 2018a, 2018b; Wan et al. 2018; Xie, Zhang, and Webster 2018; Hijazi et al. 2019; Maulik et al. 2019; Pagani, Manzoni, and Carlberg 2019).

The DDC-ROM is a hybrid projection/data-driven ROM, in which the standard Galerkin method is used to model the terms involving only the resolved modes and available data is used to model only the ROM closure term. This parsimonious/minimalistic datadriven approach is made possible by using ROM spatial filtering (i.e. ROM projection) and an LES/VMS framework to isolate the ROM closure term, which is then approximated by using data. The DDC-ROM minimalistic data-driven framework is similar in spirit to the NARMAX (Chorin and Lu 2015; Lu, Lin, and Chorin 2017) and PM (Chekroun, Liu, and Wang 2015; Chekroun, Liu, and McWilliams 2019) ROM closure models, although they differ in the way the closure terms are handled. The DDC-ROM centers around ROM spatial filtering, whereas in the NARMAX approach the closure terms are modelled using nonlinear autoregression moving average with the resolved modes as exogenous inputs, and the PM approach parameterises explicitly the unresolved modes in terms of the resolved modes.

The rest of the paper is organised as follows: In Section 2, we briefly present the QGE and the construction of the corresponding DDC-ROM. In Section 3, we assess the performance of the DDC-ROM using two metrics: the time-averaged streamfunction and the kinetic energy. Finally, in Section 4, we summarise our findings and outline future research directions.

#### 2. Data-driven correction ROM (DDC-ROM)

In this section, we present the construction of the DDC-ROM for the QGE.

#### 2.1. Quasi-geostrophic equations (QGE)

In what follows, we use the quasi-geostrophic equations (QGE) as a mathematical model:

$$\frac{\partial \omega}{\partial t} + J(\omega, \psi) - \text{Ro}^{-1} \frac{\partial \psi}{\partial x} = \text{Re}^{-1} \Delta \omega + \text{Ro}^{-1} F,$$
(10)

$$\omega = -\Delta \psi, \tag{11}$$

where  $\omega$  is the vorticity,  $\psi$  is the streamfunction, Re is the Reynolds number, and Ro is the Rossby number. As a test problem for numerical investigation, we consider the QGE (10) and (11) with a symmetric double-gyre wind forcing given by

$$F = \sin(\pi(y - 1)). \tag{12}$$

The single-layer QGE (10) and (11) (also known as a barotropic vorticity equation (BVE)), are a popular mathematical model for forced-dissipative large scale ocean circulation (Majda and Wang 2006; Vallis 2006; Cushman-Roisin and Beckers 2011). The QGE are a simplified model that allows efficient numerical simulations while preserving many of the essential features of the underlying large scale ocean flows. The QGE are similar to the streamfunction-vorticity formulation of the two-dimensional Navier Stokes equations (NSE) (Gunzburger 1989). The main difference between the two equations is that the QGE include rotation effects (due to the Coriolis force), which yield an additional term  $(-Ro^{-1}(\partial \psi/\partial x))$  and an additional parameter (Ro). The idealised double-gyre wind forcing setting has been often used to understand the wind-driven circulation, e.g. the role of mesoscale eddies and their effect on the mean circulation. ROMs for the QGE (10) and (11) have been used, e.g. in Selten (1995), Crommelin and Majda (2004), Galán del Sastre and Bermejo (2008), San and Iliescu (2015) and Strazzullo et al. (2018).

The spatial domain of the QGE is  $\Omega = [0, 1] \times [0, 2]$  and the time domain is [0, 80]. We assume that  $\psi$  and  $\omega$  satisfy homogeneous Dirichlet boundary conditions:

$$\psi(t, x, y) = 0,$$
  
 $\omega(t, x, y) = 0$  for  $(x, y) \in \partial \Omega$  and  $t \ge 0$ . (13)

The QGE (10) and (11) can be cast in the general form of the nonlinear equation (1) by choosing

$$(f(\omega), \nu) = -(J(\omega, \psi), \nu) + \text{Ro}^{-1}\left(\frac{\partial \psi}{\partial x}, \nu\right)$$
$$-\text{Re}^{-1}(\nabla \omega, \nabla \nu) + \text{Ro}^{-1}(F, \nu). \quad (14)$$

We refrain from giving the precise formulation of the functional space here since this is tangential to the numerical study carried out below. The interested readers can consult for instance (Gunzburger 1989, Chapter 11), for the case of Navier-Stokes equations in the streamfunction-vorticity formulation. We will make precise how the terms in (14) are computed numerically once a set of POD basis functions for the vorticity is computed based on the direct numerical simulation (DNS) data obtained from a spectral code; see Sections 2.2 and 3.1.

# 2.2. Standard Galerkin ROM (G-ROM)

In our investigation, the ROM basis is obtained by using the proper orthogonal decomposition (POD) (Holmes, Lumley, and Berkooz 1996; Noack, Morzynski, and Tadmor 2011). We note, however, that other bases could be used for this purpose as well; examples include the dynamic mode decomposition (Schmid 2010), the principal interaction patterns (Kwasniok 1996, 1997; Hasselmann 1988), and the HIGAMod (Perotto et al. 2017). See also (Crommelin and Majda 2004; Tu et al. 2014; Taira et al. 2017) for recent surveys and relationships/comparisons between different modal decomposition approaches.

We focus here mainly on the functional form of the G-ROM and defer details about the POD basis construction to Section 3. To this end, given an r-dimensional ROM subspace  $X^r$  spanned by the first r POD basis functions for the vorticity  $\omega$ ,

$$X^r := \operatorname{span}\{\varphi_1, \dots, \varphi_r\},\tag{15}$$

the r-dimensional G-ROM takes the form of (2) with f therein given by (14). Recall that the streamfunction  $\psi$  in (14) is related to the vorticity  $\omega$  through the Poisson equation (11) subject to homogeneous Dirichlet boundary conditions.

To further reduce the G-ROM to an explicit ODE system, one option would be to replace  $\psi$  in (14) by  $-\Delta^{-1}\omega$ , with  $\Delta^{-1}$  being the inverse of the Laplacian of  $\omega$  subject to the aforementioned boundary conditions. But since one important metric we adopt to assess the performance of the ROMs concerns the time average of  $\psi$ , we decide to keep  $\psi$  explicit in the ROM formulation, although either way would lead to the same r-dimensional ODE system. For this reason, we also introduce a reduced set of r basis functions for  $\psi$ , which are subordinate to the above POD basis functions for  $\omega$  in (15) via  $\phi_i(x,y) = -\Delta^{-1}\varphi_i(x,y)$ , i.e.

they solve the following Poisson equation:

$$-\Delta \phi_i(x, y) = \varphi_i(x, y)$$
, subject to  $\phi_i(x, y) = 0$ , for  $(x, y) \in \partial \Omega$ ,  $i = 1, 2, \dots, r$ . (16)

Note that while the POD basis  $\{\varphi_i\}$  for the vorticity  $\omega$  is an orthonormal basis under  $L^2$  inner product, the basis  $\{\phi_i\}$  for the streamfunction  $\psi$  is not orthogonal. Given the G-ROM approximation  $\omega_r = \sum_{i=1}^r a_i(t)\varphi_i(x, y)$  of  $\omega$ , the corresponding  $\psi$  is approximated by  $\psi_r =$  $\sum_{i=1}^{r} a_i(t)\phi_i(x,y)$ , which results from the ansatz  $\psi_r =$  $-\Delta^{-1}\omega_r$  and definition (16) of the basis function  $\phi_i$ .

With the above notations, the r-dimensional G-ROM for the problem (10)–(13) is given by:

$$\left(\frac{\partial \omega_r}{\partial t}, \varphi_i\right) + (J(\omega_r, \psi_r), \varphi_i) - \operatorname{Ro}^{-1}\left(\frac{\partial \psi_r}{\partial x}, \varphi_i\right) 
+ \operatorname{Re}^{-1}(\nabla \omega_r, \nabla \varphi_i) = \operatorname{Ro}^{-1}(F, \varphi_i),$$
(17)

where  $(\cdot, \cdot)$  denotes the  $L^2$  inner product over the spatial domain, and i = 1, ..., r. Plugging the vorticity and streamfunction ROM approximations in (17), yields the Galerkin ROM (G-ROM):

$$\dot{a} = b + A a + a^{\top} B a, \tag{18}$$

where  $\mathbf{a} \stackrel{def}{=} (a_j(t))_{j=1}^r$  is the vector of time-varying ROM coefficients, b is the r-dimensional vector corresponding to the forcing term, A is the  $r \times r$  matrix corresponding to the linear terms, and *B* is the  $r \times r \times r$ r tensor corresponding to the nonlinear term. The G-ROM (18) can be written componentwise as follows: for i = 1, 2, ..., r

$$\dot{a}_i(t) = b_i + \sum_{m=1}^r A_{im} a_m(t) + \sum_{m=1}^r \sum_{n=1}^r B_{imn} a_m(t) a_n(t),$$
(19)

where  $b_i = \text{Ro}^{-1}(F, \varphi_i), A_{im} = \text{Ro}^{-1}(\partial \phi_m / \partial x, \varphi_i) Re^{-1}(\nabla \varphi_m, \nabla \varphi_i), B_{imn} = -(I(\varphi_m, \varphi_n), \varphi_i).$ 

#### 2.3. DDC-ROM

To construct the DDC-ROM (8) for the QGE, we adapt the general presentation in Section 1 to the QGE setting.

For clarity of presentation, we assume that the differentiation and the ROM projection commute (see, however, Koc et al. 2019 for a detailed discussion of the commutation error). Thus, the linear terms in the QGE do not appear in the Correction term of the DDC-ROM. Next, we note that the Correction term (7) takes the following form for the QGE:

Correction = 
$$(f(\omega_R) - f(\omega_r), \varphi_i)$$
  
=  $(J(\omega_R, \psi_R) - J(\omega_r, \psi_r), \varphi_i)$   
=  $(\frac{\partial \omega_R}{\partial x} \frac{\partial \psi_R}{\partial y} - \frac{\partial \psi_R}{\partial x} \frac{\partial \omega_R}{\partial y}, \varphi_i)$   
 $-(\frac{\partial \omega_r}{\partial x} \frac{\partial \psi_r}{\partial y} - \frac{\partial \psi_r}{\partial x} \frac{\partial \omega_r}{\partial y}, \varphi_i),$  (20)

where  $\omega_R(\mathbf{x},t) = \sum_{i=1}^R a_i(t)\varphi_i(\mathbf{x})$  and  $\psi_R(\mathbf{x},t) =$  $\sum_{i=1}^{R} a_i(t)\phi_i(\mathbf{x})$  are the R-dimensional ROM approximations of the vorticity and streamfunction in  $X^R$ , respectively, and  $\mathbf{x} = (x, y)$ . We emphasise that the Correction (20) is R-dimensional instead of r-dimensional, where  $R \gg r$ . Thus, to include the Correction (20) in the DDC-ROM, we first need to find an efficient, r-dimensional approximation of the Correction. To this end, we make the following *linear* ansatz:  $\forall i = 1, \ldots, r,$ 

Correction = 
$$\left( \frac{\partial \omega_R}{\partial x} \frac{\partial \psi_R}{\partial y} - \frac{\partial \psi_R}{\partial x} \frac{\partial \omega_R}{\partial y}, \varphi_i \right)$$
$$- \left( \frac{\partial \omega_r}{\partial x} \frac{\partial \psi_r}{\partial y} - \frac{\partial \psi_r}{\partial x} \frac{\partial \omega_r}{\partial y}, \varphi_i \right)$$
$$\approx \left( g(\omega_r), \varphi_i \right)$$
$$= \left( \tilde{A} \mathbf{a} \right)_i,$$
 (21)

where the operator  $\tilde{A} \in \mathbb{R}^{r \times r}$  needs to be determined and  $(\hat{A} \mathbf{a})_i$  denotes the *i*-th component of the vector  $(\tilde{A} a)$ . The ansatz (21) is chosen to resemble the right-hand side of the G-ROM (18); we note, however, that other ansatzes are possible (Xie et al. 2018; Mohebujjaman, Rebholz, and Iliescu 2019).

To compute the entries in the operator  $\hat{A}$  in (21), we use a data-driven approach. To this end, we adapt the least squares problem (9) to the QGE setting:

$$\min_{\tilde{A}} \sum_{j=1}^{M} \left\| \left[ \left( \frac{\partial \omega_{R}}{\partial x} \frac{\partial \psi_{R}}{\partial y} - \frac{\partial \psi_{R}}{\partial x} \frac{\partial \omega_{R}}{\partial y}, \varphi_{i} \right) - \left( \frac{\partial \omega_{r}}{\partial x} \frac{\partial \psi_{r}}{\partial y} - \frac{\partial \psi_{r}}{\partial x} \frac{\partial \omega_{r}}{\partial y}, \varphi_{i} \right) \right] - \tilde{A} \mathbf{a}^{\text{DNS}}(t_{j}) \right\|^{2}.$$
(22)

In (22),  $a^{\text{DNS}}(t_i)$  is the vector of ROM coefficients obtained from the DNS data, i.e. from the snapshots, at time instances  $t_j$ ,  $j=1,\ldots,M$ , which are obtained by projecting the corresponding snapshots  $\omega^{\text{DNS}}(t_j) = \sum_{k=1}^R a_k^{\text{DNS}}(t_j) \, \varphi_k$  onto the POD basis functions  $\varphi_i$  and using the orthogonality of the POD basis functions:  $\forall i=1,\ldots,r, \ \forall j=1,\ldots,M$ ,

$$a_i^{\text{DNS}}(t_j) = \left(\omega^{\text{DNS}}(t_j), \varphi_i\right).$$
 (23)

The *data-driven correction ROM (DDC-ROM)* has the following form for the QGE:

$$\dot{a} = b + (A + \tilde{A})a + a^{\top}Ba, \tag{24}$$

where the operators b, A, and B are the G-ROM operators in (18) and the operator  $\tilde{A}$  is the solution of the least squares problem (22).

## 3. Numerical experiments

In this section, we investigate the DDC-ROM (24) in the numerical simulation of the QGE.

# 3.1. Computational setting and snapshot generation

We investigate the QGE (10) and (11) in a computational setting similar to that used in Holm and Nadiga (2003), San et al. (2011) and San and Iliescu (2015). In particular, we use the symmetric double-gyre wind forcing given in (12), homogeneous Dirichlet boundary conditions for  $\psi$  and  $\omega$  given in (13), and the parameters Re = 450 and Ro = 0.0036.

For the DNS spatial discretization, we use a spectral method with a 257  $\times$  513 spatial resolution. Since both the vorticity and streamfunction have homogeneous boundary conditions, we approximate both functions with a tensor product Sine expansion in x and y. For the DNS time discretization, we use an explicit Runge-Kutta method (Tanaka-Yamashita, an order 7 method with an embedded order 6 method for error control) and an error tolerance of  $10^{-8}$  in time with adaptive time refinement and coarsening. We record the solution values every  $10^{-2}$  simulation time units (starting at 0) regardless of the current time step size so that the snapshots used in the POD are equally spaced. These spatial and temporal discretizations yield numerical results that are similar to the fine resolution numerical results obtained in San et al. (2011) and San and Iliescu (2015). We follow

San et al. (2011) and San and Iliescu (2015) and run the DNS between [0, 80]. The time evolution of the spatially averaged kinetic energy in Figure 1 in San and Iliescu (2015) shows that, on the time interval [0, 10], the flow displays a transient behaviour that is characterised by large changes in the kinetic energy of the system. After this short transient dynamics, the flow reaches a statistically steady state on the interval [10, 80]. Capturing the complex dynamics during the initial transient phase would require a large number of ROM modes. Thus, we follow San et al. (2011) and San and Iliescu (2015) and evaluate the ROMs in the statistically steady regime, i.e. on the time interval [10, 80]. We emphasise, however, that even in the statistically steady state regime, the flow displays a high degree of variability. Thus, the numerical approximation of this statistically steady regime remains challenging for the low resolution ROMs that we investigate in this section.

#### 3.2. ROM construction

To generate the ROM basis (see Section 2), we follow San et al. (2011) and San and Iliescu (2015) and collect 701 equally spaced snapshots of the vorticity,  $\omega$ , in the time interval  $[T_{\min}, T_{\max}] = [10, 80]$  (on which the statistically steady state regime is attained) at equidistant time intervals. We also interpolate the DNS vorticity onto a uniform mesh with the resolution  $257 \times 513$ over the rectangle domain  $\Omega = [0, 1] \times [0, 2]$ , i.e. h = $\Delta x = \Delta y = 1/256$ . We then use the 701 snapshots, form the correlation matrix *C* for vorticity, and obtain the POD basis functions  $\varphi_i$ 's from the eigenvectors of C. Recall that the element  $C_{ij}$  of C is simply the  $L^2$ inner product of the i-th and the j-th snapshots, i.e.  $C_{ij} = \int_{\Omega} \omega_i \omega_j \, dx \, dy$  (San and Iliescu 2015). Throughout the article, the  $L^2$  inner product over  $\Omega$  is carried out by using the two-dimensional form of Simpson's 1/3 rule. Once the POD basis functions for the vorticity are generated, we solve the Poisson equation (16) to construct the streamfunction basis functions. For this purpose, we use a second order central difference (five-point stencil) spatial discretization of the Laplace operator.

In Figure 1, we present the contour plots of selected streamfunction basis functions  $\phi_i$ 's and vorticity POD basis functions  $\varphi_i$ 's to give an idea about how the spatial scales are organised in these computed bases as the basis function index increases. Note that  $\varphi_i$ s are much

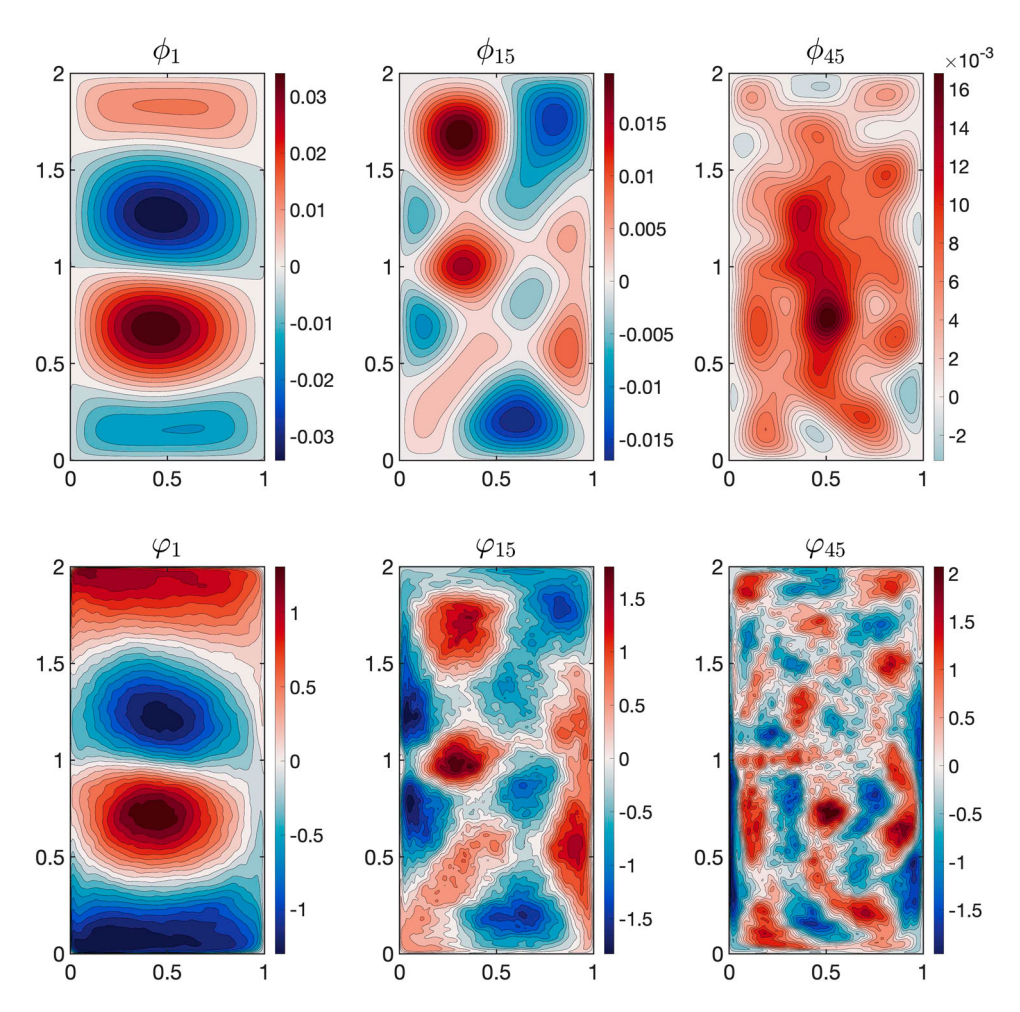


**Figure 1.** Basis functions for the streamfunction (first row) and vorticity (second row). The vorticity basis functions  $\varphi_i$ 's are the POD modes computed based on the DNS snapshots for the vorticity, while each streamfunction basis function  $\phi_i$  is related to  $\varphi_i$  via  $\phi_i = -\Delta^{-1}\varphi_i$ ; see Section 2.2.

rougher than  $\phi_i$ s, especially for the higher indices, whereas the roughness is smoothed out by the Laplacian when the  $\phi_i$ s are computed according to (16). One source of roughness could be the uniform discretization mesh adopted here (257 × 513) when interpolating the DNS data, since there are steep gradients in the vorticity field as time evolves, both near the western boundary and within the domain. However, as we will illustrate in the next section, such roughness does not significantly degrade the DDC-ROM accuracy.

To construct the DDC-ROM, we need to solve the least squares problem (22), which can be ill-conditioned, especially when the training data is relatively short with respect to the number of coefficients that need to be learnt. To tackle this ill-conditioning issue, we use the truncated singular value decomposition (SVD) (see Step 6 of Algorithm 1 in Xie et al. 2018) with a tolerance that yields the most accurate results. Furthermore, to increase the computational efficiency

of the DDC-ROM, we replace  $(\omega_R, \psi_R)$  in (22) with  $(\omega_m, \psi_m)$ , where  $r \leq m \leq R$ . As explained in Section 5.3 in Xie et al. (2018), choosing an m value close to r decreases the cost of computing  $\tilde{A}$  and  $\tilde{B}$ , but also reduces the DDC-ROM's accuracy. On the other hand, choosing an m value close to R increases the DDC-ROM's accuracy, but also increases the cost of computing  $\tilde{A}$  and  $\tilde{B}$ . Our numerical experiments suggest that m = 3r achieves a good balance between numerical accuracy and computational efficiency for the considered QGE model.

In our numerical investigation, in addition to the DDC-ROM, we also consider the *physically-constrained* DDC-ROM (CDDC-ROM) (Mohebujjaman, Rebholz, and Iliescu 2019), which aims at improving the physical accuracy of the DDC-ROM. To construct the CDDC-ROM, we add physical constraints that require that the data-driven CDDC-ROM operators satisfy the same type of physical laws as those

satisfied by the QGE. Specifically, we require that the CDDC-ROM's Correction term's linear component (i.e. the matrix  $\tilde{A}$ ) should be dissipative. To implement these physical constraints, in the data-driven modelling step, we replace the unconstrained least squares problem (22) with a constrained least squares problem:

$$\min_{\substack{\tilde{A} \in \mathbb{R}^{r \times r} \\ \boldsymbol{a}^{\top} \tilde{A} \, \boldsymbol{a} \leq 0}} \sum_{j=1}^{M} \left\| \left[ \left( \frac{\partial \omega_{R}}{\partial x} \frac{\partial \psi_{R}}{\partial y} - \frac{\partial \psi_{R}}{\partial x} \frac{\partial \omega_{R}}{\partial y}, \varphi_{i} \right) - \left( \frac{\partial \omega_{r}}{\partial x} \frac{\partial \psi_{r}}{\partial y} - \frac{\partial \psi_{r}}{\partial x} \frac{\partial \omega_{r}}{\partial y}, \varphi_{i} \right) \right] - \tilde{A} \, \boldsymbol{a}^{\text{DNS}}(t_{j}) \right\|^{2}.$$
(25)

Additionally, we also monitor the commutation error, which represents the effect of interchanging ROM spatial filtering and differentiation (Koc et al. 2019). For this test problem, modelling the commutation error does not significantly change the DDC-ROM and CDDC-ROM results, suggesting that the commutation error does not play a significant role in the ROM construction. Thus, for clarity of presentation, we do not include the commutation error in the DDC-ROM and CDDC-ROM results.

In the online stage, for all the ROMs we utilise the fourth order Runge-Kutta scheme (RK4) for the temporal discretization. To ensure the numerical stability of the time discretization, we choose a time step size  $\Delta t = 0.001$ . We store ROM data every ten time steps to match the DNS sampling rate. We use the DNS snapshot at t = 10 to initialise the ROMs.

#### 3.3. Numerical results

In this section, we present numerical results for the G-ROM, DDC-ROM, and CDDC-ROM. As a benchmark for our numerical investigation, we use the DNS results.

#### 3.3.1. Kinetic energy

In this section, we assess the performance of the ROMs using the DNS kinetic energy as a metric. As pointed out in Section 1, due to the involvement of a broad range of active spatial scales, it would be too demanding to require any ROMs to reproduce the statistics of the DNS kinetic energy or any other reasonable observables when the dimension is too low, at least within the POD basis framework adopted here. Thus, we confine ourselves instead to a much less ambitious

goal of reproducing the range of oscillations presented in the DNS kinetic energy. The assessment at a more quantitative level will be carried out in the next section for another metric.

Recall that the velocity field  $(u(\mathbf{x},\cdot),v(\mathbf{x},\cdot))$  used in the computation of the kinetic energy  $E(t)=\frac{1}{2}\int_{\Omega}(u^2(\mathbf{x},t)+v^2(\mathbf{x},t))\,\mathrm{d}\mathbf{x}$  is related to the streamfunction according to  $(u,v)=(\partial_y\psi,-\partial_x\psi)$ . The first-order spatial derivatives are calculated using a 4-th order accurate central difference scheme. The kinetic energy itself is computed using the two-dimensional form of Simpson's 1/3 rule.

In Figure 2, for three different r values (r = 10, 15, and 40), we plot the time evolution of the ROM kinetic energy. For r = 10, the G-ROM kinetic energy takes off very quickly and stabilises at a level around  $8 \times 10^4$ , which is roughly 200 times higher than the DNS kinetic energy on average. In contrast, both the DDC-ROM and CDDC-ROM successfully stabilise the G-ROM, and produce kinetic energies almost of the same order of magnitude as the DNS kinetic energy (although there is some overdamping in the CDDC-ROM result due to the physical constraint  $\mathbf{a}^{\top}\tilde{A}$   $\mathbf{a} \leq 0$ ; see (25)).

For r=15, the G-ROM kinetic energy is within good range at the beginning of the simulation, but increases to an unphysical value around t=40 and eventually stabilises and oscillates around  $2 \times 10^4$ . In contrast, the DDC-ROM and CDDC-ROM kinetic energies are both within the good range, and between the two, the CDDC-ROM performs better in reproducing the peaks and the corresponding frequency of the peaks.

Finally, for r = 40, the G-ROM and DDC-ROM perform similarly. The DDC-ROM kinetic energy is closer to the DNS kinetic energy over certain time windows (e.g. [50, 60]), whereas the CDDC-ROM kinetic energy is somewhat lower than the DNS kinetic energy.

The above results suggest that both the DDC-ROM and CDDC-ROM can successfully stabilise a severely truncated G-ROM. For the chosen criterion, the advantage of the DDC-ROM over the G-ROM is clearly visible for all ROM dimensions r between 10 and 30. The CDDC-ROM can produce results comparable or even better than DDC-ROM for r between 10 and 20. For even higher dimensions, the CDDC-ROM tends to overdamp the kinetic energy. This is plausible, since the physical constraint  $\mathbf{a}^{\mathsf{T}}\tilde{\mathbf{A}}\mathbf{a} \leq 0$  in

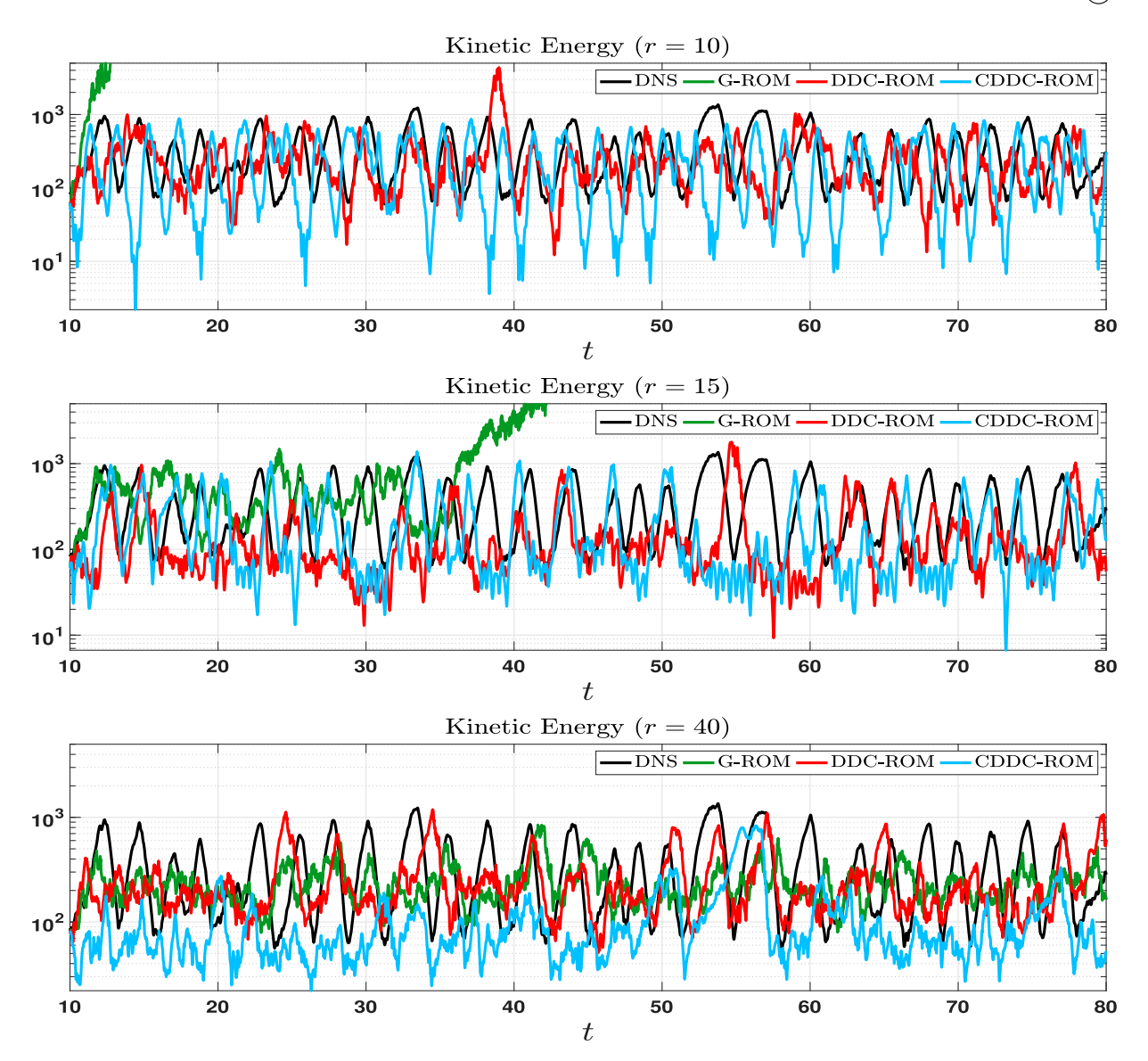


**Figure 2.** Kinetic energy of DNS, G-ROM, DDC-ROM and CDDC-ROM with different r values. All the ROMs are initialised at t=10 using the projected DNS data.

the estimation of the matrix  $\tilde{A}$  for the CDDC-ROM aims to enhance the stability of the ROM, but does not also guarantee improved accuracy compared to the DDC-ROM.

# 3.3.2. Relative errors for the time-averaged streamfunction

In this section, we assess the ROM performance at a more quantitative level using the ROM time-averaged streamfunction over the aforementioned time interval, [10, 80]. It is known that the time-averaged streamfunction displays a four-gyre structure (Greatbatch and Nadiga 2000) even though a double-gyre wind forcing is employed; cf. (12). The metric that we use

is the following relative error:

$$\left\| \overline{\psi^{\text{DNS}}(\mathbf{x}, \cdot)} - \overline{\psi^{\text{ROM}}(\mathbf{x}, \cdot)} \right\|_{L^{2}}^{2} / \left\| \overline{\psi^{\text{DNS}}(\mathbf{x}, \cdot)} \right\|_{L^{2}}^{2}, \tag{26}$$

where  $\overline{(\cdot)}$  represents time average over [10, 80], and  $\mathbf{x} = (x, y)$ .

In Table 1, we list this relative error for each of the ROMs as the ROM dimension r increases. For small r values (i.e.  $5 \le r \le 20$ ), the CDDC-ROM is the most accurate. Indeed, for r=5, the CDDC-ROM is the only ROM that yields a stable approximation: all other ROMs with r=5 experience exponential blowup with the given timestep. Furthermore, for r=10 and r=15, the CDDC-ROM error is

**Table 1.** The relative errors for the time-averaged streamfunction defined by (26).

r values	G-ROM	DDC-ROM	CDDC-ROM
r = 5	n/a	n/a	5.07e+00
r = 10	2.06e+02	3.25e-01	9.58e-02
r = 15	3.05e+02	2.83e-01	1.03e-01
r = 20	5.05e+00	1.39e-01	1.20e-01
r = 25	1.73e+00	1.61e-01	2.96e-01
r = 30	1.47e+00	1.18e-01	4.58e-01
r = 35	6.83e-01	1.34e-01	7.69e-01
r = 40	4.69e-01	9.17e-02	4.92e-01
r = 45	2.81e-01	4.16e-02	6.83e+00
r = 50	3.66e-01	8.20e-02	4.16e-01

at most half of the DDC-ROM error. Finally, for  $5 \le r \le 50$ , the G-ROM error is one to three orders of magnitude larger than the CDDC-ROM error. These results are also supported by the plots in Figure 3, which display the time-average of the streamfunction  $\psi$  over the time interval [10, 80] for DNS, G-ROM (r = 10), DDC-ROM (r = 10), and CDDC-ROM (r = 10). These plots clearly show that the DDC-ROM and CDDC-ROM are able to capture the correct four-gyre structure, whereas the G-ROM fails drastically at this low ROM dimension.

For large r values (i.e.  $25 \le r \le 50$ ), the DDC-ROM results in Table 1 are the most accurate. Indeed, at r = 25 the CDDC-ROM error starts to increase, whereas the DDC-ROM error generally decreases. The G-ROM error also continues to decrease, but it is always larger than the DDC-ROM error.

We conclude that the CDDC-ROM is the most accurate for small r values and the DDC-ROM is the most accurate for large r values. These results suggest that adding physical constraints to the DDC-ROM is beneficial in the highly truncated cases (i.e. for small r values), but the benefit brought by the physical constraints diminishes as r is further increased, and can even produce less accurate results than DDC-ROM due to overdamping, as pointed out in Section 3.3.1. We emphasise, however, that we are using the linear ansatz to construct the DDC-ROM; further numerical investigations are needed to determine the role of physical constraints when the DDC-ROM is built with a higher-order (e.g. quadratic) ansatz (Mohebujjaman, Rebholz, and Iliescu 2019). We also note that the G-ROM is consistently less accurate than the DDC-ROM for all the r values. Finally, we note that, as r increases, the errors for all the ROMs reach a plateau instead of converging to zero. We believe that this behaviour is due to the roughness present in the vorticity basis functions, especially for the higher indices (see Figure 1).

### 3.3.3. Shorter training time interval

In this subsection, we consider the situation when the ROMs are trained on a time interval that is shorter than the time interval over which the ROMs are tested. Specifically, we only use snapshots in the time interval [10,  $t_n^*$ ], sampled every 0.1 time units as before, to generate the ROM basis and construct the ROM operators A, B, and A. This leads to a total number of  $(t_p^* -$ 10)/0.1 + 1 snapshots. We investigate two different cases: (I)  $t_p^* = 45$  and (II)  $t_p^* = 35$ .

In Table 2, we list the relative errors associated with the ROMs for the time-averaged streamfunction defined in (26). The results show that the DDC-ROM is significantly more accurate than the G-ROM, especially for small r values. Moreover, for small r values,

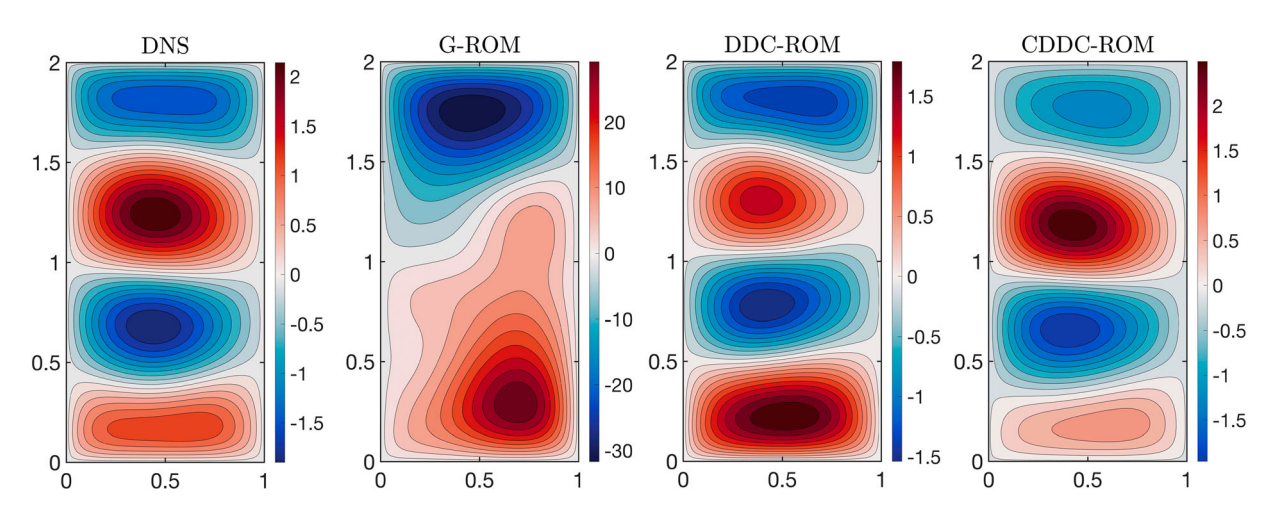


**Figure 3.** Time-averaged streamfunction  $\psi$  over the interval [10, 80] for DNS, 10-dim G-ROM, 10-dim DDC-ROM, and 10-dim CDDC-ROM.

**Table 2.** The ROM relative errors for the time-averaged streamfunction defined in (26) for the two predictive test cases: the POD basis functions are generated using DNS snapshots over the time interval [10, 45] for Case I and over [10, 35] for Case II. The ROM simulations are carried out in the time interval [10, 80].

	Predictive Case I				Predictive Case II		
r values	G-ROM	DDC-ROM	CDDC-ROM	G-ROM	DDC-ROM	CDDC-ROM	
r = 5	n/a	n/a	1.83e+01	n/a	n/a	3.40e-01	
r = 10	1.39e+04	3.33e-01	2.43e-01	1.91e+02	6.56e-01	4.44e-01	
r = 15	9.58e+00	3.76e-01	1.69e-01	1.94e+01	3.27e-01	8.18e-02	
r = 20	5.37e+00	1.35e-01	3.47e-01	6.35e+00	1.80e-01	2.25e-01	
r = 25	2.28e+00	9.47e-02	3.66e-01	1.44e+00	3.05e-01	4.81e-01	
r = 30	5.65e-01	1.32e-01	7.70e-01	5.27e-01	1.96e-01	6.25e-01	
r = 35	2.88e-01	1.76e-01	6.03e-01	2.26e-01	1.71e-01	6.27e-01	
r = 40	2.07e-01	1.72e-01	6.92e-01	2.44e-01	2.20e-01	6.56e-01	
r = 45	2.86e-01	2.15e-01	5.74e-01	3.20e-01	2.34e-01	7.04e-01	
r = 50	1.67e-01	2.09e-01	5.87e-01	3.53e-01	2.72e-01	5.61e-01	

the CDDC-ROM is more accurate than the DDC-ROM, whereas for larger r values, the DDC-ROM is more accurate than the DDC-ROM. This is in line with the results in Sections 3.3.1 and 3.3.2. Furthermore, we note that, as expected, the shorter the time interval  $[10, t_p^*]$  is, the larger the ROM relative error.

#### 4. Conclusions

We enhanced the standard Galerkin ROM (G-ROM) for the quasi-geostrophic equations (QGE) with an additional term derived from available data and a least squares optimisation procedure. These ideas are based on previous work and are usually referred to as data-driven correction ROMs (DDC-ROMs) and constrained data-driven correction ROMs (CDDC-ROMs). The latter incorporate a negative semidefiniteness constraint into the optimisation problem to preserve a fundamental property of the linear operator in the DDC-ROMs.

The QGE are challenging equations that exhibit complex spatiotemporal behaviour: we were able to significantly improve the G-ROM performance by adding an additional term (derived by optimisation) to the linear component of the G-ROM. For a ROM with 10 POD modes, the DDC-ROM lowered the error in the mean streamfunction (compared to the G-ROM) by a factor of about 600; similarly, the CDDC-ROM lowered the error by a factor of about 2000.

In the future, we plan on investigating whether using a higher-order (e.g. quadratic) ansatz in the construction of the DDC-ROM and CDDC-ROM yields more accurate results than using a linear ansatz (i.e. the approach utilised in this paper). We also plan to study parameter sensitivity (on both the Reynolds

and Rossby numbers) and examine the possibility of constructing a sequence of ROMs that work across a wide range of each value.

#### Note

1. Subject to possible further integration by parts for certain terms in (f(u), v).

# **Acknowledgments**

The authors are grateful to the two anonymous referees for their insightful and constructive comments.

#### **Disclosure statement**

No potential conflict of interest was reported by the authors.

## **Funding**

This work is partially supported by National Science Foundation (NSF) DMS-1821145 (CM,TI), NSF DMS-1616450 (HL), and NSF DMS-1450327 (DRW).

#### References

Azaïez, M., T. C. Rebollo, and S. Rubino. 2017. "Streamline Derivative Projection-Based POD-ROM for Convection-Dominated Flows. Part I: Numerical Analysis." arXiv preprint http://arxiv.org/abs/1711.09780.

Baiges, J., R. Codina, and S. Idelsohn. 2015. "Reduced-Order Subscales for POD Models." *Computer Methods in Applied Mechanics and Engineering* 291: 173–196.

Ballarin, F., E. Faggiano, S. Ippolito, A. Manzoni, A. Quarteroni, G. Rozza, and R. Scrofani. 2016. "Fast Simulations of Patient-Specific Haemodynamics of Coronary Artery Bypass Grafts Based on a POD–Galerkin Method and a Vascular Shape Parametrization." *Journal of Computational Physics* 315: 609–628.



- Bergmann, M., C. H. Bruneau, and A. Iollo. 2009. "Enablers for Robust POD Models." Journal of Computational Physics 228 (2): 516-538.
- Brunton, S. L., and J. N. Kutz. 2019. Data-driven Science and Engineering: Machine Learning, Dynamical Systems, and Control. Cambridge: Cambridge University Press.
- Chekroun, M. D., and D. Kondrashov. 2017. "Data-Adaptive Harmonic Spectra and Multilayer Stuart-Landau Models." Chaos: An Interdisciplinary Journal of Nonlinear Science 27: 093110.
- Chekroun, M. D., H. Liu, and J. C. McWilliams. 2019. "Variational Approach to Closure of Nonlinear Dynamical Systems: Autonomous Case." Journal of Statistical Physics. doi:10.1007/s10955-019-02458-2.
- Chekroun, M. D., H. Liu, and S. Wang 2015. Stochastic Parameterizing Manifolds and Non-Markovian Reduced Equations: Stochastic Manifolds for Nonlinear SPDEs II. Springer Briefs in Mathematics, New York: Springer.
- Chorin, A. J., and F. Lu. 2015. "Discrete Approach to Stochastic Parametrization and Dimension Reduction in Nonlinear Dynamics." Proceedings of the National Academy of Sciences 112: 9804-9809.
- Couplet, M., C. Basdevant, and P. Sagaut. 2005. "Calibrated Reduced-Order POD-Galerkin System for Fluid Flow Modelling." Journal of Computational Physics 207 (1): 192-220.
- Crommelin, D. T., and A. J. Majda. 2004. "Strategies for Model Reduction: Comparing Different Optimal Bases." Journal of the Atmospheric Sciences 61: 2206-2217.
- Cushman-Roisin, B., and J. M. Beckers. 2011. Introduction to Geophysical Fluid Dynamics: Physical and Numerical Aspects. New York: Academic Press.
- Fick, L., Y. Maday, A. T. Patera, and T. Taddei. 2018. "A Stabilized POD Model for Turbulent Flows Over a Range of Reynolds Numbers: Optimal Parameter Sampling and Constrained Projection." Journal of Computational Physics 371: 214-243.
- Galán del Sastre, P., and R. Bermejo. 2008. "Error Estimates of Proper Orthogonal Decomposition Eigenvectors and Galerkin Projection for a General Dynamical System Arising in Fluid Models." Numerische Mathematik 110 (1): 49-81.
- Galletti, B., C. H. Bruneau, L. Zannetti, and A. Iollo. 2004. "Low-Order Modelling of Laminar Flow Regimes Past a Confined Square Cylinder." Journal of Fluid Mechanics 503: 161-170.
- Greatbatch, R. J., and B. T. Nadiga. 2000. "Four-Gyre Circulation in a Barotropic Model with Double-Gyre Wind Forcing." Journal of Physical Oceanography 30 (6): 1461-1471.
- Gunzburger, M. D. 1989. Finite Element Methods for Viscous Incompressible Flows: A Guide to Theory, Practice, and Algorithms. Computer Science and Scientific Computing, Boston, MA: Academic Press Inc.
- Gunzburger, M., N. Jiang, and M. Schneier. 2017. "An Ensemble-Proper Orthogonal Decomposition Method for the Nonstationary Navier-Stokes Equations." SIAM Journal on Numerical Analysis 55 (1): 286-304.
- Hasselmann, K. 1988. "PIPs and POPs: The Reduction of Complex Dynamical Systems Using Principal Interaction and

- Oscillation Patterns." Journal of Geophysical Research: Atmospheres 93 (D9): 11015-11021.
- Hesthaven, J. S., G. Rozza, and B. Stamm. 2015. Certified Reduced Basis Methods for Parametrized Partial Differential Equations. New York: Springer.
- Hijazi, S., G. Stabile, A. Mola, and G. Rozza. 2019. "Data-Driven POD-Galerkin Reduced Order Model for Turbulent Flows." arXiv preprint arXiv:1907.09909.
- Holm, D. D., and B. T. Nadiga. 2003. "Modeling Mesoscale Turbulence in the Barotropic Double-Gyre Circulation." Journal of Physical Oceanography 33 (11): 2355-2365.
- Holmes, P., J. L. Lumley, and G. Berkooz. 1996. Turbulence, Coherent Structures, Dynamical Systems and Symmetry. Cambridge: Cambridge University Press.
- Koc, B., C. Mou, M. Mohebujjaman, and T. Iliescu. 2019. "Commutation Error in Reduced Order Modeling of Fluid Flows." arXiv preprint, http://arxiv.org/abs/1810.00517.
- Kondrashov, D., M. D. Chekroun, and P. Berloff. 2018. "Multiscale Stuart-Landau Emulators: Application to Wind-Driven Ocean Gyres." Fluids 3 (1): 21.
- Kondrashov, D., M. D. Chekroun, and M. Ghil. 2015. "Data-Driven Non-Markovian Closure Models." Physica D: Nonlinear Phenomena 297: 33-55.
- Kravtsov, S., D. Kondrashov, and M. Ghil. 2005. "Multilevel Regression Modeling of Nonlinear Processes: Derivation and Applications to Climatic Variability." Journal of Climate 18: 4404-4424.
- Kwasniok, F. 1996. "The Reduction of Complex Dynamical Systems Using Principal Interaction Patterns." Physica D: Nonlinear Phenomena 92 (1-2): 28-60.
- Kwasniok, F. 1997. "Optimal Galerkin Approximations of Partial Differential Equations Using Principal Interaction Patterns." Physical Review E 55 (5): 5365.
- Loiseau, J.-C., and S. L. Brunton. 2018. "Constrained Sparse Galerkin Regression." *Journal of Fluid Mechanics* 838: 42–67.
- Lu, F., K. K. Lin, and A. J. Chorin. 2017. "Data-Based Stochastic Model Reduction for the Kuramoto-Sivashinsky Equation." Physica D: Nonlinear Phenomena 340: 46-57.
- Majda, A. J., and J. Harlim. 2012. "Physics Constrained Nonlinear Regression Models for Time Series." Nonlinearity 26 (1): 201.
- Majda, A. J., and X. Wang. 2006. Nonlinear Dynamics and Statistical Theories for Basic Geophysical Flows. Cambridge: Cambridge University Press.
- Maulik, R., A. Mohan, B. Lusch, S. Madireddy, and P. Balaprakash. 2019. "Time-Series Learning of Latent-Space Dynamics for Reduced-Order Model Closure." arXiv preprint, http://arxiv.org/abs/1906.07815.
- Mohebujjaman, M., L. G. Rebholz, and T. Iliescu. 2019. "Physically-Constrained Data-Driven Correction for Reduced Order Modeling of Fluid Flows." International Journal for Numerical Methods in Fluids 89 (3): 103-122.
- Noack, B. R., M. Morzynski, and G. Tadmor. 2011. Reduced-Order Modelling for Flow Control. Vol. 528. New York: Springer Verlag.
- Noack, B. R., P. Papas, and P. A. Monkewitz. 2005. "The Need for a Pressure-Term Representation in Empirical Galerkin

- Models of Incompressible Shear Flows." *Journal of Fluid Mechanics* 523: 339–365.
- Pagani, S., A. Manzoni, and K. Carlberg. 2019. "Statistical Closure Modeling for Reduced-Order Models of Stationary Systems by the ROMES Method." arXiv preprint, http://arxiv.org/abs/1901.02792.
- Parish, E. J., C. Wentland, and K. Duraisamy. 2019. "The Adjoint Petrov-Galerkin Method for Non-Linear Model Reduction". arXiv:1810.03455v3.
- Peherstorfer, B., and K. Willcox. 2016. "Data-Driven Operator Inference for Nonintrusive Projection-Based Model Reduction." Computer Methods in Applied Mechanics and Engineering 306: 196–215.
- Perotto, S., A. Reali, P. Rusconi, and A. Veneziani. 2017. "HIG-AMod: A Hierarchical IsoGeometric Approach for MODel Reduction in Curved Pipes." *Computers & Fluids* 142: 21–29.
- Quarteroni, A., A. Manzoni, and F. Negri. 2015. *Reduced Basis Methods for Partial Differential Equations: An Introduction*. Vol. 92. New York: Springer.
- Rebollo, T. C., E. D. Ávila, M. G. Mármol, F. Ballarin, and G. Rozza. 2017. "On a Certified Smagorinsky Reduced Basis Turbulence Model." SIAM Journal on Numerical Analysis 55 (6): 3047–3067.
- San, O., and T. Iliescu. 2015. "A Stabilized Proper Orthogonal Decomposition Reduced-Order Model for Large Scale Quasigeostrophic Ocean Circulation." Advances in Computational Mathematics 41 (5): 1289–1319.
- San, O., and R. Maulik. 2018a. "Extreme Learning Machine for Reduced Order Modeling of Turbulent Geophysical Flows." *Physical Review E* 97 (4): 042322.
- San, O., and R. Maulik. 2018b. "Neural Network Closures for Nonlinear Model Order Reduction." *Advances in Computational Mathematics* 44 (6): 1717–1750.
- San, O., A. E. Staples, Z. Wang, and T. Iliescu. 2011. "Approximate Deconvolution Large Eddy Simulation of a Barotropic Ocean Circulation Model." *Ocean Modelling* 40: 120–132.
- Sapsis, T. P., and P. F. J. Lermusiaux. 2009. "Dynamically Orthogonal Field Equations for Continuous Stochastic

- Dynamical Systems." *Physica D: Nonlinear Phenomena* 238 (23-24): 2347–2360.
- Schmid, P. J. 2010. "Dynamic Mode Decomposition of Numerical and Experimental Data." *Journal of Fluid Mechanics* 656: 5–28
- Selten, F. M. 1995. "An Efficient Description of the Dynamics of Barotropic Flow." *Journal of the Atmospheric Sciences* 52 (7): 915–936.
- Strazzullo, M., F. Ballarin, R. Mosetti, and G. Rozza. 2018. "Model Reduction for Parametrized Optimal Control Problems in Environmental Marine Sciences and Engineering." SIAM Journal on Scientific Computing 40 (4): B1055–B1079.
- Taira, K., S. L. Brunton, S. Dawson, C. W. Rowley, T. Colonius, B. J. McKeon, O. T. Schmidt, S. Gordeyev, V. Theofilis, and L. S. Ukeiley. 2017. "Modal Analysis of Fluid Flows: An Overview." AIAA Journal 55 (12): 4013–4041.
- Tu, J. H., C. W. Rowley, D. M. Luchtenburg, S. L. Brunton, and J. N. Kutz. 2014. "On Dynamic Mode Decomposition: Theory and Applications." *Journal of Computational Dynamics* 1: 391–421.
- Vallis, G. K. 2006. Atmospheric and Oceanic Fluid Dynamics: Fundamentals and Large-Scale Circulation. Cambridge: Cambridge University Press.
- Wan, Z. Y., P. Vlachas, P. Koumoutsakos, and T. Sapsis. 2018. "Data-Assisted Reduced-Order Modeling of Extreme Events in Complex Dynamical Systems." *PLoS One* 13 (5): e0197704.
- Wang, Z., I. Akhtar, J. Borggaard, and T. Iliescu. 2012. "Proper Orthogonal Decomposition Closure Models for Turbulent Flows: A Numerical Comparison." Computer Methods in Applied Mechanics and Engineering 237-240: 10-26.
- Xie, X., M. Mohebujjaman, L. G. Rebholz, and T. Iliescu. 2018. "Data-Driven Filtered Reduced Order Modeling of Fluid Flows." SIAM Journal on Scientific Computing 40 (3): B834–B857.
- Xie, X., G. Zhang, and C. G. Webster. 2018. "Data Driven Reduced Order Modeling of Fluid Dynamics Using Linear Multistep Network." arXiv preprint http://arxiv.org/abs/1809.07820.